Engineered Science
DOI: https://dx.doi.org/10.30919/es1017

Thermal Management of Prismatic $LiFePO_4$ Battery Module with Inversed-Zigzag Channeled Ferrofluid Flows

Sarawut Sirikasemsuk,[1] Ponthep Vengsungnle,[2] Smith Eiamsa-ard[3] and Paisarn Naphon[4,*]

Abstract

The thermal management of battery modules plays a crucial role in their lifetime, performance, and safety risks. Overload, or external heat, gives rise to thermal runaway. Under high operational conditions, the electrolyte inside the battery cell evaporates and produces a higher pressure, causing the electrolyte to decompose, leak, ignite, and explode. The thermal behavior of the battery with the flow of ferrofluid channeled zigzag through the battery casing is considered using the turbulent mixture. The computational domain comprises twelve prismatic $LiFePO_4$ battery cells with four cooling flow jacket configurations. A reasonable agreement is reached from the comparison process. The outlet coolant temperatures for the TiO_2 nanofluids and Fe_3O_4 ferrofluids are higher than for water as the working fluid and higher concentration give increased heat removal ability. The inversed-zigzag channeled flow decreases the battery temperature. The maximum temperature gradients of the battery module are 5.00 °C, 4.60 °C, 4.53 °C, 3.41 °C, and 1.85 °C for models I, II(a), II(b), III, and IV, respectively. Therefore, this cooling system may be an alternative for designing a cooling system for the interior area of the battery module, especially a large-scale module.

Keywords: Prismatic battery; Thermal behavior; Ferrofluids; Cooling system; Thermal runaway.
Received: 18 October 2023; Revised: 06 November 2023; Accepted: 08 November 2023.
Article type: Research article.

1. Introduction

1.1 Energy density and efficiency of the battery

Pb-Acid was applied as the backbone for EV in the first few days, usually separated into starting and deep-cycle batteries.[1] However, the early EVs required many batteries, increasing the weight. It uses deep cycle types because it has higher energy capacity and sustainability. The battery does not generate a voltage; we call it a storage battery.[2] The specific power is battery charging capacity, which should have little specific energy.[3] Higher specific energy means that the motor requires more energy. The Li-ion batteries are lighter and smaller in scale than other types, facilitating their entry into the marketplace. Ni-MH is used in many applications because of its higher specific power and density.[4] Furthermore, the specific power is 40% more than Ni-Cd HEV batteries. However, due to specific power limitations, it can be as much as 75 Wh/kg.[5] Efficient energy storage is presented as the content charged and discharged from the battery. Among all types of the same size, the Li-ion battery has a greater energy density than other batteries.

1.2 Battery cooling techniques

The Battery Thermal Management System (BTMS) is crucial in modern electric vehicles because it can handle extreme operating conditions effectively. Fig. 1 shows a conceptual BTMS workflow created by the NREL to simulate the general EV battery thermal management processes and output thermal responses.[6] For the battery module, the appropriate operating condition of each battery cell is controlled by BTMS.[7] During

[1] *Department of Mechanical Engineering, Faculty of Engineering and Architecture, Rajamangala University of Technology Suvarnabhumi, Ayutthaya, 13000, Thailand.*
[2] *Department of Agricultural Machinery Engineering, Faculty of Engineering and Architecture, Rajamangala University of Technology Isan, Nakhonratchasima 30000, Thailand.*
[3] *Department of Mechanical Engineering, Faculty of Engineering, Mahanakorn University of Technology, Bangkok, 10530, Thailand.*
[4] *Thermo-Fluids and Heat Transfer Enhancement Research Lab. (TFHT), Department of Mechanical Engineering, Faculty of Engineering, Srinakharinwirot University, 63 Rangsit-Nakhornnayok Rd., Ongkharak, Nakhorn-Nayok, 26120, Thailand.*
**Email:* paisarnn@g.swu.ac.th (P. Naphon)

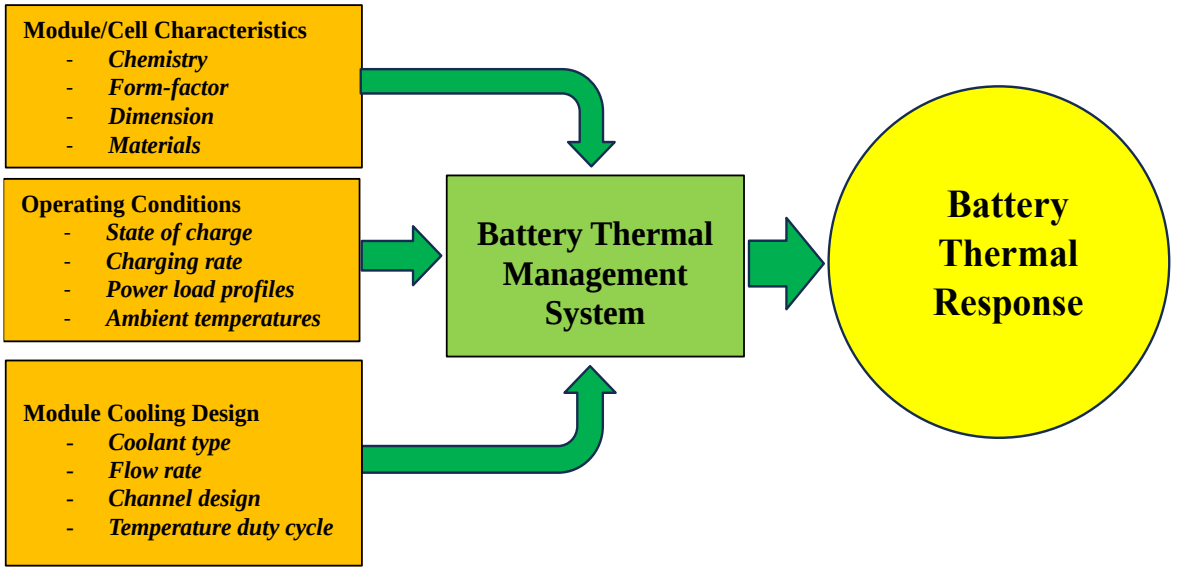

Fig. 1 Conceptual BTMS workflow by NREL.[6]

the operation, the chemical reaction process generates heat,[8] so the thermal cooling system is essential, which also depends on the cell configurations.[9] EVBs rely heavily on battery cells as their core component. The automotive industry frequently uses three cell formats: Cylindrical, pouch, and prismatic (see Fig. 2). The main distinction among cell formats is the cell casing design and the placement of the cathode, anode, and separators. Prismatic and cylindrical cells are usually packed into a hard aluminum or stainless steel case. Aluminum composite foils with multilayers are used for packaging pouch cells. A jelly roll is formed by electrode webs wound with separators in cylindrical cells. Flat jelly rolls or stacked electrodes are the primary methods for prismatic cells. Stack arrangement is the only arrangement used in pouch cells. Literature describing the Li-on battery's effectiveness, life cycle, and safety is reviewed.[10] Air cooling is a simple, uncomplicated technology where the air circulates through the system. The early-stage EV models usually adopt a passive ambient air-cooling strategy due to its compactness and low cost. It also saves more energy for the lower specific energy battery cells[11] than other technologies. Still, the limitation of this method is the thermophysical properties for removing thermal cooling. The researchers developed an air-cooling system that forces/induces air to move through the cooling devices under different conditions, which results in the cooling system's inability to control the temperature consistently during operation.[12] However, this cooling method can be modified and developed for higher cooling efficiency by different pipe geometries and airflow paths.[13,14] The relevant parameter effects, including; battery cell size and coolant flow channels on thermal cooling efficiency and thermal behavior, have been considered.[15-17] An algorithm to monitor load status (SOC), health status (SOH), load status (SOC), current, and temperature[18] has been developed. Pagaria *et al*.[19] applied

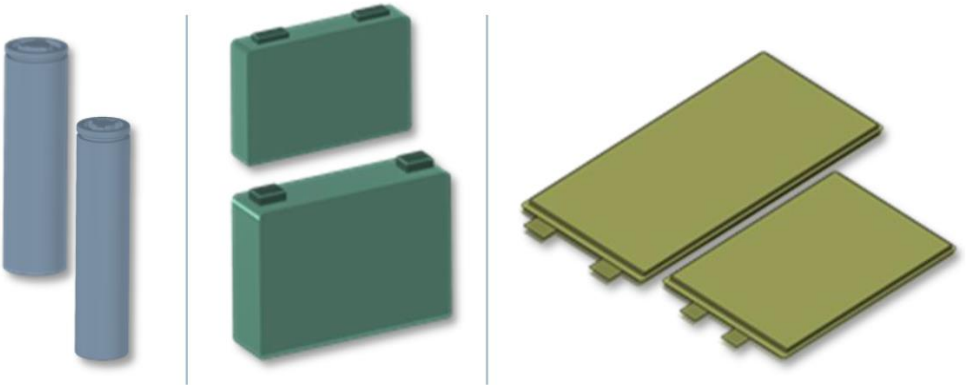

Fig. 2 Configurations of cell for (a) cylindrical cells, (b) prismatic cells, and (c) pouch cells.

a smarter battery management system and charging for electric vehicles. In addition, the thermal management systems, temperature distribution, and effect of electrodes with carbon materials on the safety of the batteries have been reviewed.[20-22]

For the liquid cooling system, water and oil have been applied as working fluids circulating in the system.[23] An EV liquid-cooling usually consists of tubes, a water pump, a heater (heat exchanger from the high-temperature engine coolant), and air conditioning (AC, which is usually used as a part of the heating, ventilation, and air conditioning system on the EV to control the cabin environment and is partially used for cooling the coolant), heat exchanger, fan, and heat transfer structures between tube and battery cells. The majority of this cooling system, the evacuation of heat, is the heat transfer through a jacket,[24] a tube,[25] and a heat sink.[26] Furthermore, the effects of geometries and cooling surface structures on thermal cooling efficiency have been examined.[27,28] The impact of various cooling channels and temperature distribution has also been studied.[29,30] The effect of C-rate, 1 C-rate means a fully charged 1 A in an hour, on the battery pack performance has been considered.[31] The work introduced the thermoelectric application for battery pack cooling with nanofluid/water as the coolant, have also been carried out.[32-36]

Another cooling technique, a latent mode for removing heat load, is known as phase change material (PCM). The phase change material (PCM) commonly used for battery thermal management is paraffin wax. Its cost is low and cheap and easily available without much change in temperature during the phase change PCM releases or absorbs a large amount of latent heat during the phase change without much temperature change. This method is a lightweight system that provides constant heat dissipation.[37] However, one of the drawbacks of this method is the restriction of the properties of the coolant. Work on embedding these methods with a cooling plate, flat tube, heat sink, and PCM was examined.[38-43] Next, Choudhari *et al*.[44] analyzed the battery thermal cooling performance with PCMs. It is important to note that machine learning models have been developed.[45] Karimi *et al*.[46] reviewed the battery cooling techniques with PCMs. Next, Cao *et al*.[47] proposed the PCM for battery pack cooling. In addition, the studies on the thermal cooling performance enhancement of the PV/T using PCM have been reviewed.[48] The heat produced by the chemical reaction had an essential impact on energy capacity and efficiency. Depending on the operation conditions, the cell's highest temperature and temperature gradient design the battery cooling system within the expected temperature range. Numerous cooling techniques are used in a battery cooling system, which has different advantages and disadvantages. The heat transferability depends on the coolant's thermophysical properties and flow conditions. Water and oil are mostly used in liquid cooling systems. Besides, ferrofluid applications as a coolant in heat transfer augmentation thermal devices have received much attention. Ferrofluid has the capability of heat transfer enhancement. The prismatic battery cells are larger than the cylindrical shape. As it is assembled into a set of modules, it has a large scale, which results in temperature distribution. This is because the inside of the battery module is not chilled, which causes heat concentration in the area. The liquid coolant channel is the essential part of a liquid-cooling system to transfer the heat from battery cells to the water tank or the environment. The design improvements for the coolant channels mainly focus on increasing the heat transfer efficiency. The purpose of this study is to consider the thermal behavior of the prismatic battery module using the channeled ferrofluids. Due to excellent chemical and physical stability and safe material, the spherical shape Fe_3O_4 nanoparticles with purity>99.9% are used for this study. The cooling system with different flow arrangements is designed and fabricated for the battery module. In addition, the effects of the coolant types and ferrofluids concentration on the maximum battery module temperature and outlet coolant temperatures have been investigated.

2. Mathematical modeling

2.1 The main governing equations

The combined convection of a nanofluid composed of nanoparticles (Fe_3O_4) suspended in the base fluid (Water) in the jacket of the battery cooling module was considered. The geometries and dimensions of the problem are illustrated in Fig. 3, and the details of the prismatic $LiFePO_4$ cell are shown in Table 1. The mixture model is used in the simulation process, assuming a high-phase coupling, and the particles closely follow the flow, which is supposed to have the velocity interaction of both phases. The governing equations for each phase in the mixture are used separately, and this model provides good predictions for nanofluid problems.[49,50] The mixture model uses the following assumptions:

- No phase changes have taken place.
- Single pressure is taken into account for all phases.
- Interactions between individual scattered phases are excluded.
- It does not include the generation of secondary turbulence.
- The secondary phase significantly directly impacts turbulence in the primary phase.

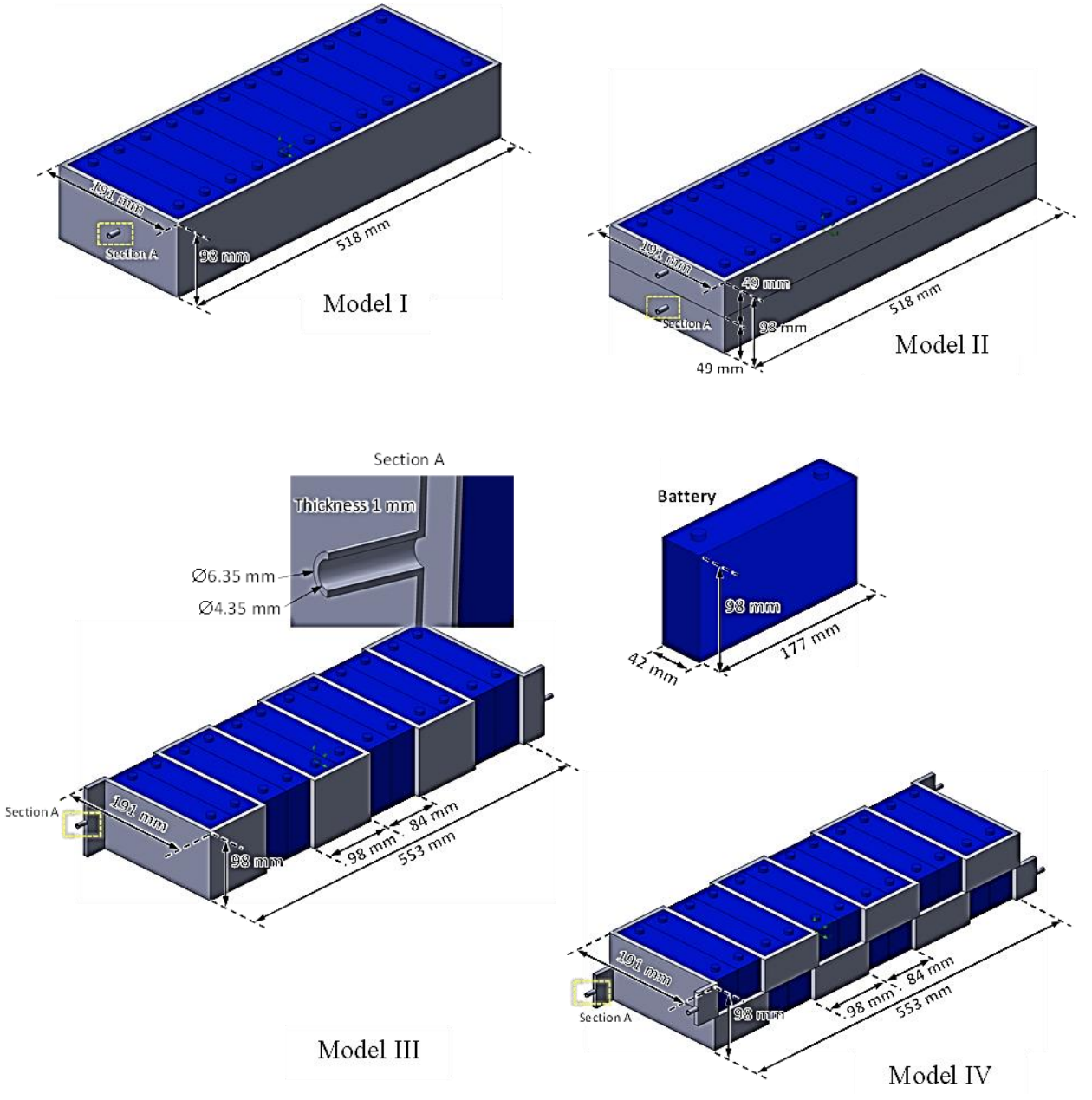

Fig. 3 Dimension of the battery module.

Table 1. Details of the prismatic $LiFePO_4$ battery.

Properties	Specification
Electrolyte material chemistry	Lithium Iron Phosphate
Dimension (Width*Length*High)	42*177*98 mm
Weight	1395 g
Nominal capacity	50 Ah
Nominal voltage	3.2 V
Charge cut-off voltage	3.65V (100% SOC)
Discharge cut-off voltage	2.50V (0% SOC)
Number of cells	12
Total voltage	38.4 V

2.1.1 Battery

The energy conservation of the module batteries may be written as follows:

$$\nabla \cdot (\lambda_b \nabla T_b) + Q = 0 \quad (1)$$

where ρ_b, $C_{p,b}$, and λ_b are the battery cell's density, heat capacity, and thermal conductivity, respectively. T_b is the cell temperature, and Q is the heat in the battery cell. The heat from the battery can be calculated from Bernardi[51] as follows:

$$Q = I(\boldsymbol{V} - \boldsymbol{V}_{OCV}) + IT\frac{d\boldsymbol{V}_{OCV}}{dT} \quad (2)$$

where $I(\boldsymbol{V}\text{-}\boldsymbol{V}_{OCV})$ is the irreversible heat mode (Ohmic and polarization heat), I is the supplied current, $\boldsymbol{V}_{OCV}$ is the open-circuit battery voltage, $\boldsymbol{V}$ is the voltage provided, T is the battery temperature. The second term is reversible heat change due to entropy change. The entropy coefficient ($d(\boldsymbol{V}_{OCV})/dT$) is dependent on the relevant parameters (Energy density, state of charge, battery temperature).[51] Reversible heat mode

predominates at low intensity, and irreversible heat at high intensity.[52] Both the charged and discharged processes significantly affect the irreversible increase in heat.[53]

2.1.2 Coolant

The principal equations that describe the flow of the mixing fluid and the heat transfer characteristics in the battery cooling module jacket are:[54]

Continuity equation:

$$\nabla \cdot (\rho_m V_m) = 0 \tag{3}$$

Momentum equation:

$$\nabla \cdot (\rho_m V_m V_m) = -\nabla p_m + \nabla(\mu_m \nabla V_m) + \nabla \cdot \left(\sum_{k=1}^{n} \phi_k \rho_k V_{dr,k} V_{dr,k}\right) - \rho_m \beta_m g(T - T_i) \tag{4}$$

The density of the mixture may be calculated from.[55]

$$\rho_m = (1 - \phi)\rho_w + \phi \rho_p \tag{5}$$

where ϕ is the volume fraction

Energy equation:

$$\nabla \cdot \sum_{k=1}^{n} \left(\phi_k V_k C_{pk} T\right) = \nabla \cdot (\lambda_m \nabla T) \tag{6}$$

Volume fraction:

$$\nabla \cdot \left(\phi_p \rho_p V_m\right) = -\nabla \cdot \left(\phi_p \rho_p V_{dr,p}\right) \tag{7}$$

The viscosity of the mixture may be calculated from.[56]

$$\mu_m = (1 + 2.5\phi)\mu_w \tag{8}$$

The mixture's thermal conductivity may be determined from.[57]

$$\lambda_m = \left[\frac{\lambda_p + 2\lambda_w - 2\phi(\lambda_w - \lambda_p)}{\lambda_p + 2\lambda_w + \phi(\lambda_w - \lambda k_p)}\right] \lambda_w \tag{9}$$

The specific heat of the mixture may be calculated from.[58]

$$\left(\rho C_p\right)_m = \phi\left(\rho C_p\right)_p + (1 - \phi)\left(\rho C_p\right)_w \tag{10}$$

V_m is the average mass velocity:

$$V_m = \frac{\sum_{k=1}^{n} (\phi_k \rho_k V_k)}{\rho_m} \tag{11}$$

$V_{dr,k}$ is the secondary drift velocity.

$$V_{dr,k} = V_{pw} - \sum_{k=1}^{n} \frac{\phi_k \rho_k}{\rho_m} V_k \tag{12}$$

Manninen *et al.*[59] and Schiller *et al.*[60] proposed the relative velocity and drag function, respectively, as follows:

$$V_{pw} = \frac{\rho_p d_p^2}{18 \mu_w f_{drag}} \frac{(\rho_p - \rho_m)}{\rho_p} (g - (V_m \cdot \nabla) V_m) = V_p - V_w \tag{13}$$

$$f_{drag} = \begin{cases} 1 + 0.15\, Re_p^{0.687} & Re \le 1000 \\ 0.0183\, Re_p & Re > 1000 \end{cases} \tag{14}$$

The k–e turbulence model for the mixture is expressed as follows:[61]

Turbulent kinetic energy (k) equation:

$$\nabla \cdot (\rho_m V_m k) = \nabla \cdot \left(\frac{\mu_{t,m}}{\sigma_k} \nabla k\right) + G_{k,m} - \rho_m \varepsilon \tag{15}$$

Turbulent kinetic energy dissipation (ε) equation:

$$\nabla \cdot (\rho_m V_m \varepsilon) = \nabla \cdot \left(\frac{\mu_{t,m}}{\sigma_\varepsilon} \nabla \varepsilon\right) + \frac{\varepsilon}{k}\left(C_1 G_{k,m} - C_2 \rho_m \varepsilon\right) \tag{16}$$

Where

$$\mu_{t,m} = \rho_m C_\mu \frac{k^2}{\varepsilon} \tag{17}$$

$$G_{k,m} = \mu_{t,m}(\nabla V_m + (\nabla V_m)^T) \tag{18}$$

The constants are obtained from the comprehensive data fitting as follows:[61]

$$C_\mu = 0.09,\ C_1 = 1.44,\ C_2 = 1.92,\ \sigma_k = 1.0,\ \sigma_\varepsilon = 1.3 \tag{19}$$

2.1.3 The cell battery and aluminum cooling block interface

The heat transfer between the battery and the cooling jacket is obtained as follows:

$$-\lambda_b \frac{\partial T}{\partial n} = -\lambda_{al} \frac{\partial T}{\partial n} \tag{20}$$

Where λ_b and λ_{al} are the cell thermal conductivity and cooling jacket, $\frac{\partial T}{\partial n}$ is the temperature gradient across the object in the normal direction.

2.1.4 The cooling jacket and working fluid interface

The interface between the cooling jacket and the coolant is defined by:

$$-\lambda_{al} \frac{\partial T}{\partial n} = h_c(T_{al} - T_{coo}) \tag{21}$$

Where h_c is the convective heat transfer coefficient between the coolant and the cooling jacket surface, T_{al} and T_{coo} are the temperatures of the cooling jacket and coolant, respectively.

2.2 Boundary conditions

The calculation process was conducted under the following conditions:

- Exterior wall: adiabatic.
- Inlet: $T = T_{in}, V = V_{in}$
- Outlet: $p_{out} = o$
- Battery wall: $q = q_{in}$

2.3 Numerical simulation and verification

Nanofluids with Fe_3O_4 nanoparticle[62] suspension are prepared ultrasonically with a constant nanoparticle concentration of 0.015% per volume without surfactants, with details as shown in Table 2. As mentioned above, the thermophysical properties of ferrofluid used in the numerical process can be calculated from the proposed correlation. SIMPLEC algorithm[63] is employed to deal with the model using the Ansys Fluent (2022). The computational domains of the problems are shown in Fig. 4. The ferrofluids circulate in the cooling jacket of the prismatic battery module. All grid configurations of the

numerical analysis are depicted in Fig. 5. There are three approaches to non-uniform processes for grid independence to ensure the accuracy of results. As shown in Table 3, outlet coolant temperatures independent of the grid number have a value > 8,900,000 for model II and >9,000,000 for model IV. The grid numbers of 8,900,000 (model II) and 9,000,000 (model IV) are adequate for the precision of the predicted results. The diagnostic computing system includes 18 CPU cores and 96 GB of RAM. The computation process ends when the rest reaches the cut-off value ($<10^{-5}$).

Table 2. Thermo-physical properties of nanoparticle (Fe_3O_4).[62]

Properties	Values at 25±1
Density, (kg/m^3)	5180
Thermal conductivity, (W/m.K)	80.4
Viscosity, (mPa S)	-
Specific heat, (J/kg.K)	670
Purity, %	>99.9
Average diameter, nm	23

Table 3. Grid-independent test for model III and model IV.

Grids (model II)	Outlet temperature (°C)	% Error
2,100,000	27.77	
8,900,000	27.43	1.22
10,900,000	27.40	0.11
Grids (model IV)	**Average outlet temperature (°C)**	**% Error**
5,400,000	27.65	
9,000,000	27.34	1.12
10,800,000	27.33	0.04

This section focuses on verifying intended outcomes. The turbulent mixture model considered the flow and thermal behaviors of a nanofluid circulating through the jacket of the battery cooling module. There are no experimental results for the battery cooling model as indicated in Fig. 3. However, we attempted to confirm the predicted results of the turbulent mixture model by using it to analyze the battery cooling system according to the published work[32] and compared with the predicted results of the Eulerian model.[46] The predicted results from the present study are in good agreement with measured data[32] and give an error of 4.93%, and reasonable

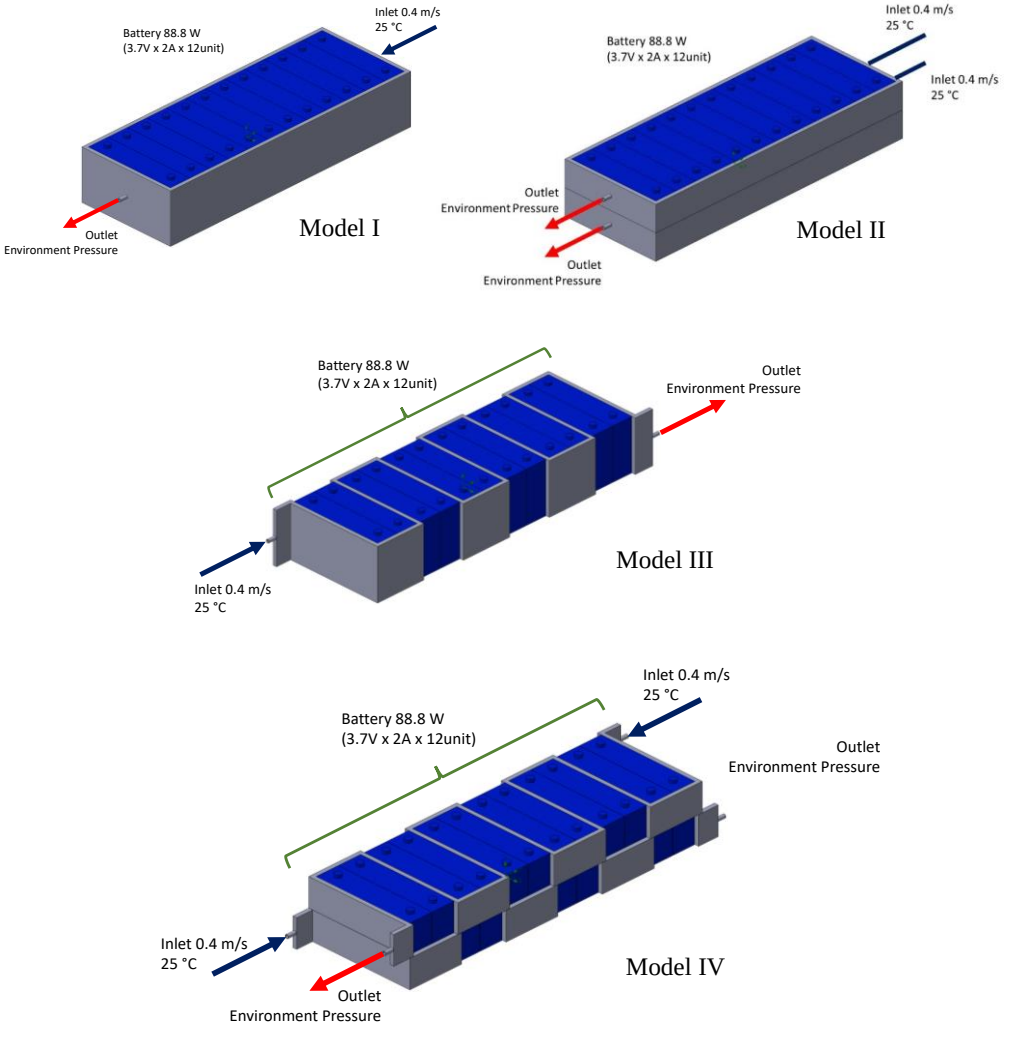

Fig. 4 Computational domain for the numerical analysis.

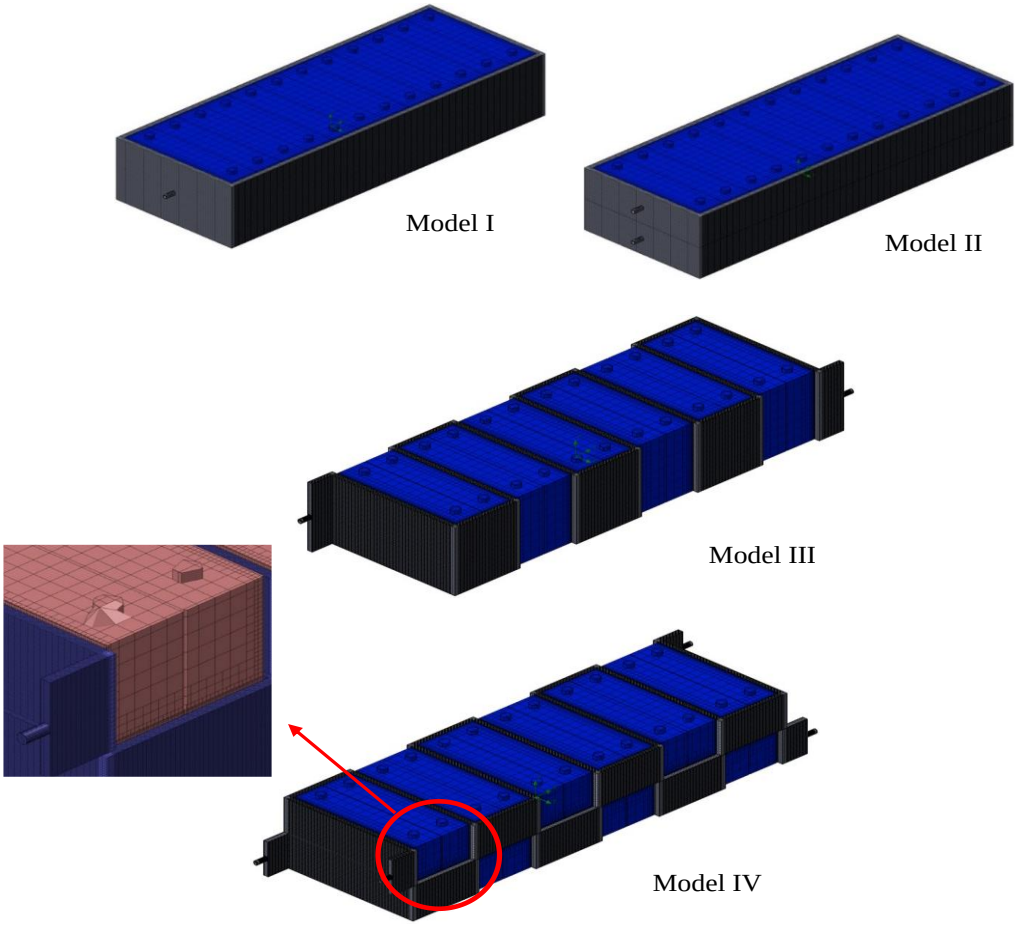

Fig. 5 Grid configuration used in the numerical analysis.

agreement with predicted results from the Eulerian model[46] as shown in Table 4. In addition, the maximum battery temperature obtained is consistent with the study.[64]

Table 4. Comparison of the outlet coolant temperature from the measured data,[32] the predicted results from [46], and the present predicted results.

Cooling models[32]	Outlet coolant temperature (°C)			% Error
	Measured data[32]	Predicted results[46]	Present predicted results	
Case I	28.72	29.77	28.34	1.33
Case II	26.32	28.71	27.65	4.93

3. Results and discussion

The thermal distribution and flow characteristics of the prismatic $LiFePO_4$ battery module for different cooling flow jacket configurations, coolant types, and coolant concentrations are analyzed and presented. The mixture model analyzes the thermal characteristics of the inversed zigzag-channeled ferrofluid flow through the battery housing. For the cylindrical battery cell assembled into a set of modules, there is rarely a problem with heat concentration, and the temperature difference within the same cell exceeds the acceptable standard. This is because the battery cells are small and cylindrical in shape. However, the prismatic battery cells are larger than the cylindrical shape. As it is assembled into a set of modules, the thermal dissipation design is not good; it causes the heat spot at the internal zone, and the temperature difference across the cell exceeds the acceptable value, negatively affecting the battery module's performance and long life. This study presents the battery cooling system for the prismatic $LiFePO_4$ battery module with a single and double-layer flow channel of the outer cold plate cooling system with different coolants and concentrations. The suspension of nanoparticles in the base fluid alters the transfer properties of the working fluid. Higher flow disturbance near the wall significantly increases the swirling flow, resulting in higher turbulent intensity and higher nanoparticle mixing. Therefore, the ability to remove heat using nanofluids as a coolant is higher than using water as a coolant. The Fe_3O_4 ferrofluids give the battery module cooling ability higher than TiO_2 nanofluids for providing the same concentration. At higher concentrations of nanofluids, as a result of greater surface area and molecular collisions, energy transport tends to increase with the concentrations of nanofluids. Therefore, a

higher level of nanofluids increases the heat transfer rate, as shown in Tables 5 and 6. For the operating conditions, a very low voltage (trickle) is set for the charging process and a 4A current rate for the discharging process. In addition, the single and double-layer inversed zigzag flow channels with ferrofluid flowing through the system are proposed. The thermal distribution of the outer cold plate for the battery module is shown in Fig. 6. The coolant flows into the system at the middle zone of the battery module, then bifurcates and flows along the outer surface of the battery module. After that, they converge in the manifold at the outlet port on the other side of the battery module. From the considering system, heat is transferred from the battery module to the coolant flowing through the flow channels around the battery module. It is found that the outer zone around the battery has the lowest temperature and tends to increase continuously and then has the highest value in the inner zone, about 30.26 °C at the 4th cell from the exit port. Moreover, the temperature of the packaging is observed to increase downstream. The maximum temperature gradient (maximum-minimum) of the battery modules is about 5 °C, and the maximum temperature gradient across the cell is 2.24 °C. Considering the coolant, it was found that the temperature continuously increases and has a maximum value of about 28.59 °C at the exit port, as shown in Fig. 6.

Table 5. Effect of coolant types on the temperatures of the battery module (model IV).

Temperature (°C)	Coolant types		
	Water	TiO_2 nanofluids	Fe_3O_4 ferrofluids
Average outlet coolant	26.02	26.15	26.18
Maximum battery module	27.45	27.23	27.17

Table 6. Effect of ferrofluid concentrations on the temperatures of the battery module (model IV).

Temperature (°C)	Ferrofluids concentration (%by volume)		
	0.010	0.015	0.020
Average outlet coolant	26.15	26.18	26.23
Maximum battery module	27.24	27.13	26.95

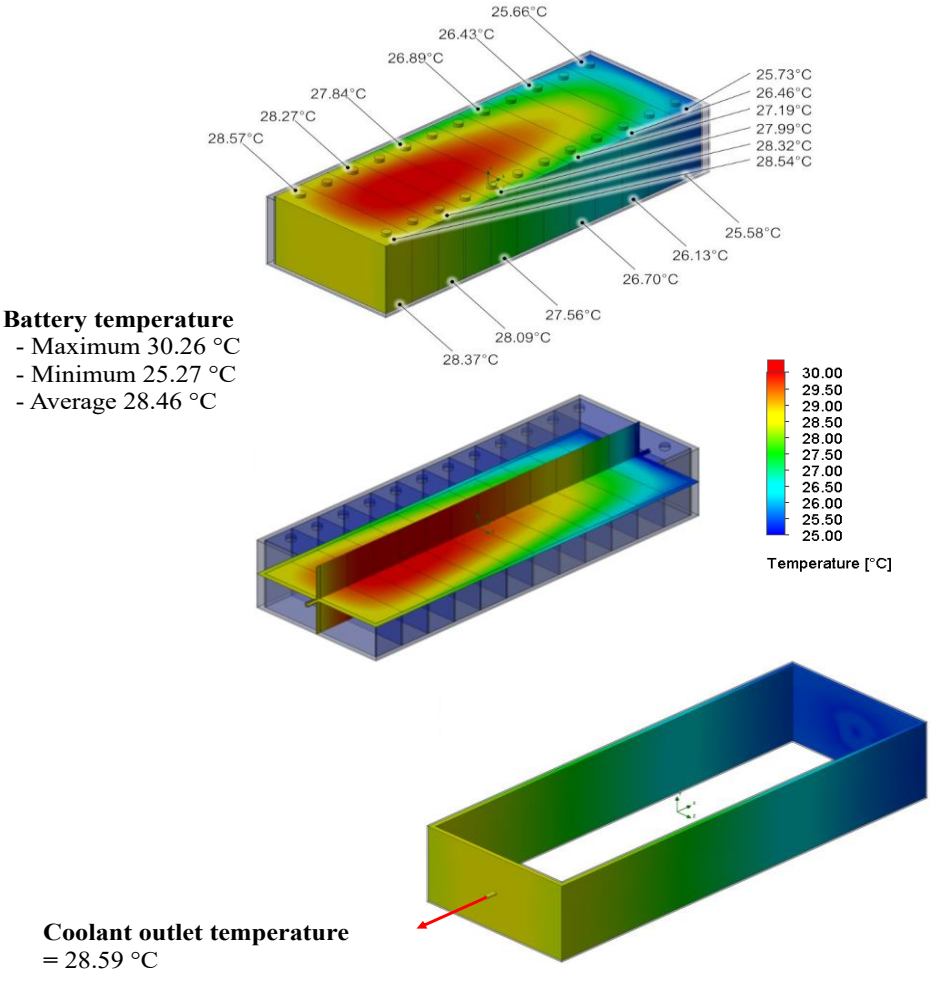

Fig. 6 Variations of the battery module and coolant temperatures (Model I).

To reduce the highest temperature of the cell, we designed the cooling system as a two-flow channel (upper and lower), as shown in Fig. 7. Fig. 7 shows the temperature of model II with the same coolant flow direction. It was found that the temperature distribution characteristics of the battery modules were similar to model I, but the highest temperature from model II(a) is less than that of model I. The maximum temperature of 30.02 °C is in the inner region of the battery (4th cell from the output port). The temperature gradients of the battery module and across the cell are 4.60 °C and 2.22 °C, respectively. The effect of the coolant flow direction on the battery module's temperature distribution is illustrated in Fig. 8. The first flow enters the cooling jacket at the top end and a second current at the bottom end. The highest temperature of the battery module occurs at the center of the inside, about 29.88 °C, and tends to decrease slightly as the outer zone. The highest temperature gradients of the pack and across the cell are 4.53 and 2.13 °C, respectively.

The thermal management system is crucial in their lifetime, performance, and safety risks. The results from models I and II, the temperature gradient of the battery module and across the cell is still high. This is because the inside of the battery module is not chilled. The optimum working temperature for a battery pack is 15 °C to 35 °C. The optimal temperature gradient must be less than 5 °C to avoid adverse reactions.[65] A battery management system (BMS) is included in most lithium-ion batteries to prevent the battery from operating beyond a specified temperature threshold. If the battery temperature exceeds this threshold, the anodic coating decomposes. At high operating conditions, the electrolyte starts to evaporate, and the pressure in the cell increases, which can cause the battery to fail mechanically. The heat increases the reaction rate, increasing its temperature and resulting in a sequence of exothermal chemical reactions inside each cell. The uncontrolled increase in temperature and pressure in the battery causes the electrolyte to break down, leak, ignite, and explode.

The thermal runaway can be initiated, causing a domino

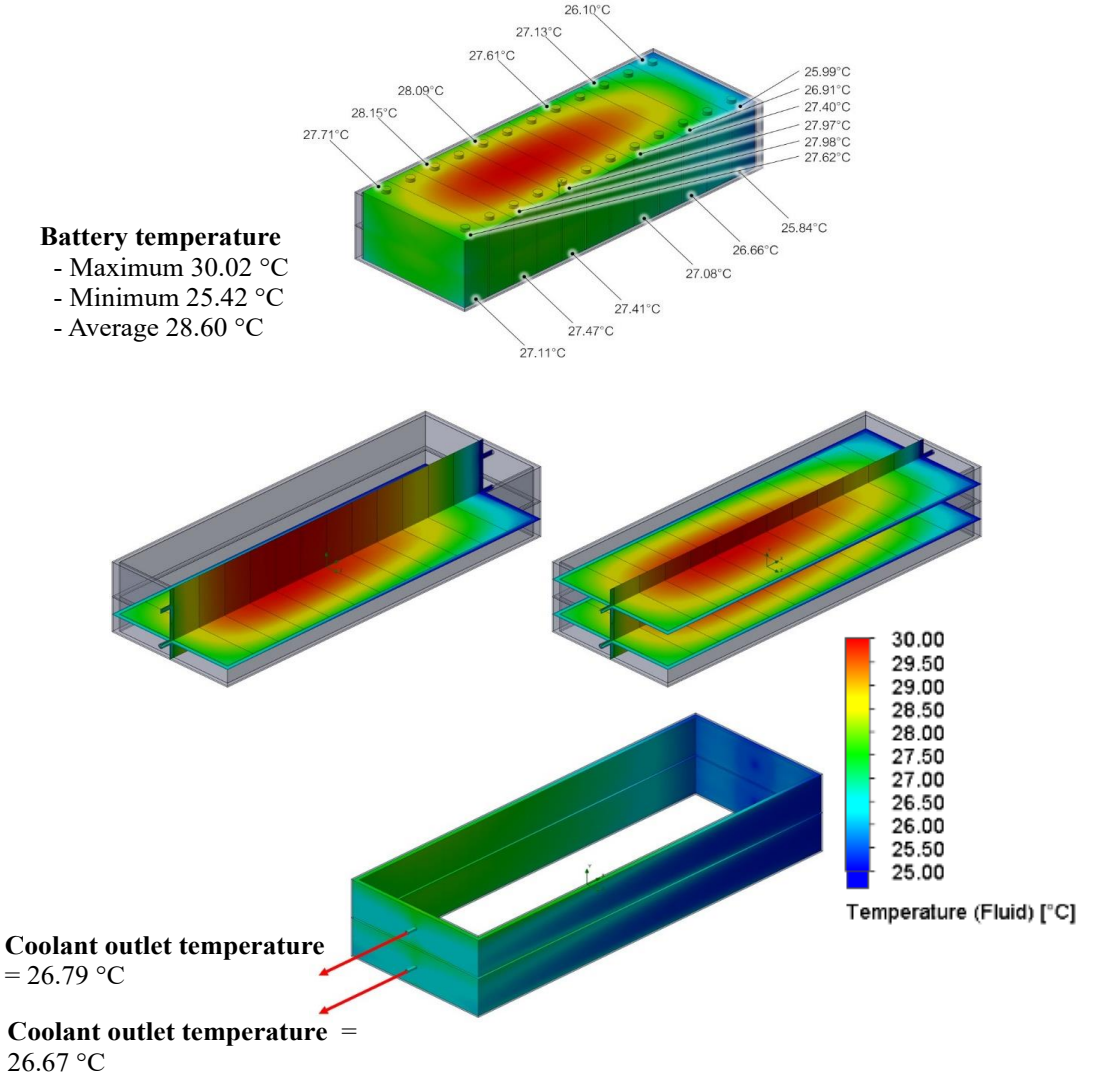

Fig. 7 Variations of the battery module and coolant temperatures for co-current flow (Model II(a)).

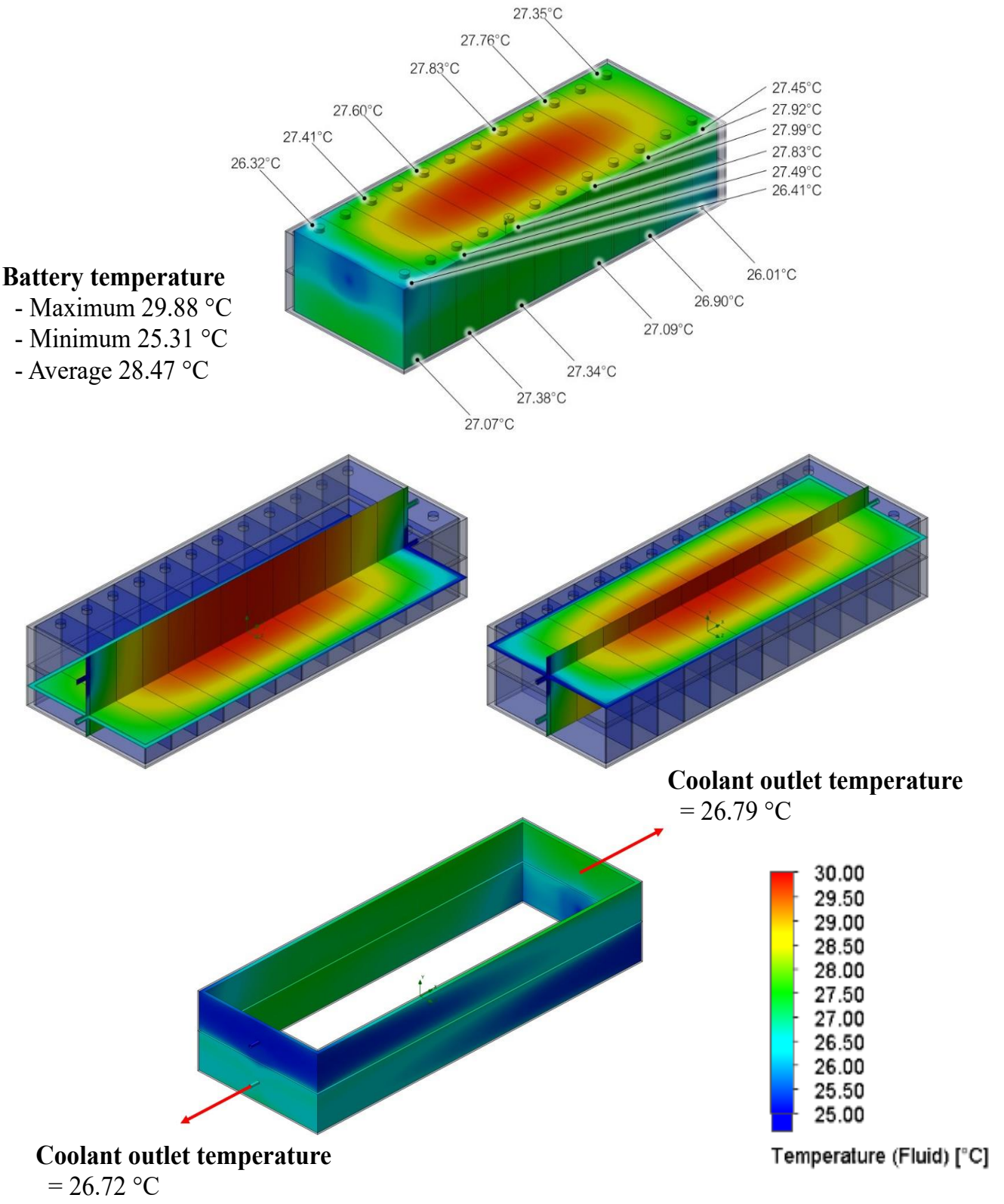

Fig. 8 Variations of the battery module and coolant temperatures for countercurrent flow (Model II(b)).

effect until each cell of the battery is degraded, which overcharging, short-circuiting, or the presence of external heat causes the thermal runaway. Therefore, a battery cooling system that can cool the internal zone is proposed, as shown in models III and IV. The inversed-zigzag cooling system is shown in Fig. 9. Cooling fluid enters the system at the front end of the middle area. After that, it follows along the zigzag flow channel that can chill the central area of the pack and then exits the system at the other end. The lowest temperature occurs in the coolant inlet area, which rises continuously when

the distance from the inlet is greater.

A maximum value at the last cell at the outlet zone is about 28.67 ºC, which is the maximum temperature obtained with Model III is lower than that obtained with Models I, II. Furthermore, the heat concentration occurs at the outlet zone of the pack. Unlike models 1 and 2, heat is concentrated in the central region. The highest temperature gradient of the pack is 3.41 ºC, and the highest temperature gradient of a single cell is 0.85 ºC.

Reducing the pack's highest temperature and temperature difference can be obtained by dividing the flow into two streams, and the flow characteristic is opposite, as in Fig. 10. The first mainstream enters the pack at the front lower flow channel. In contrast, another mainstream enters at the other end (upper flow channel). This flow arrangement reduces the concentration of heat at the downstream zone. The figure shows that the highest temperature of 27.13 °C occurs at the upper zone of the pack, and the highest temperature gradient across the battery module is 1.85 °C, as shown in Fig. 10. The variations of ferrofluid temperature along the flow channel for models I and IV are presented in Fig. 11. It is found that the coolant temperature tends to increase with increasing distance from the inlet port which corresponds to the change in the battery module temperature. The effect of the coolant flow rate on the battery module temperature is shown in Fig. 12. Based on model IV, the removal cooling ability of coolant increases with increasing flow rate. We found that the highest temperature for the highest flow rate is 26.73 ºC, followed by a moderated flow rate of 26.38 ºC and the lowest flow rate of 26.27 ºC.

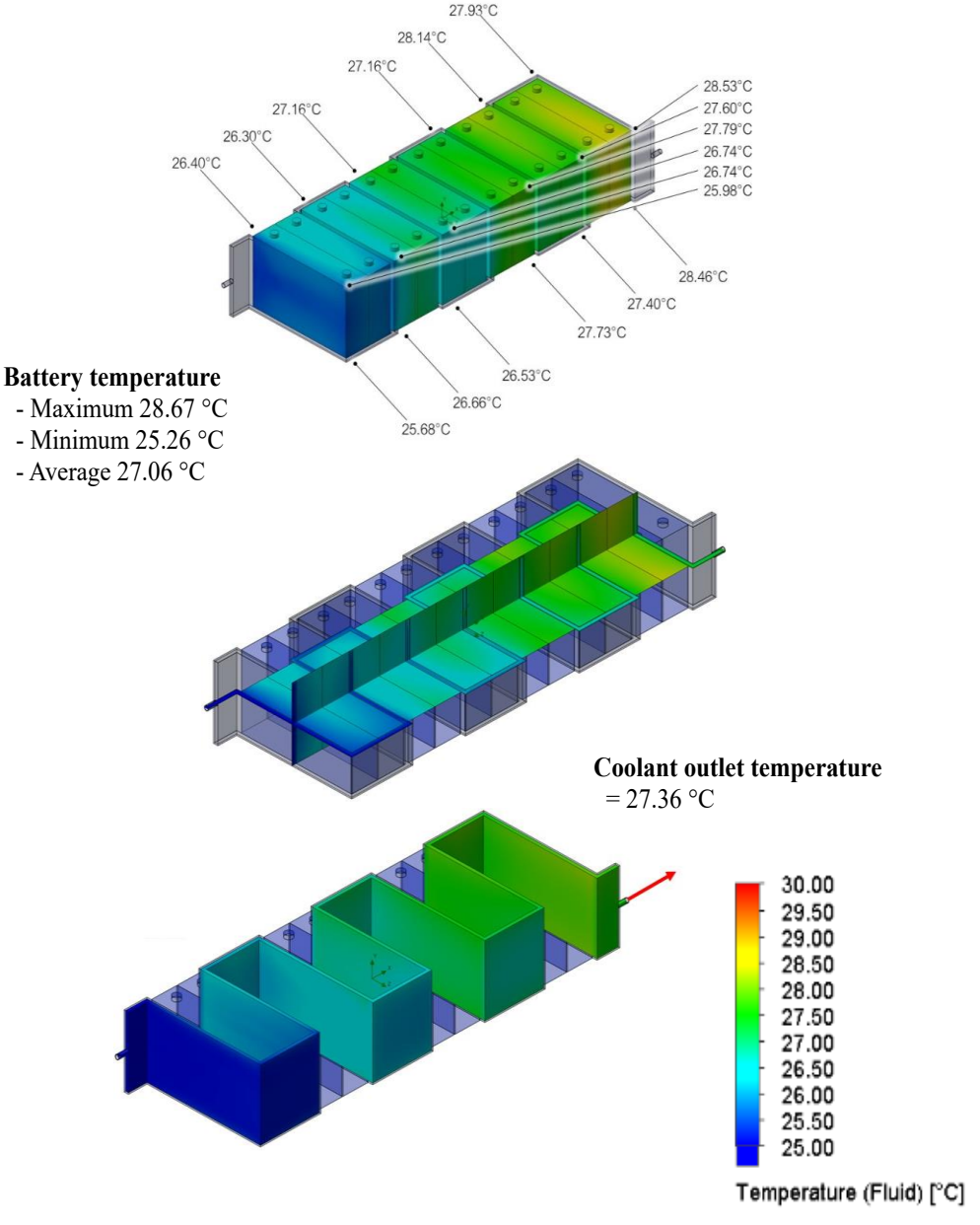

Fig. 9 Variations of the battery module and coolant temperatures for co-current flow (Model III).

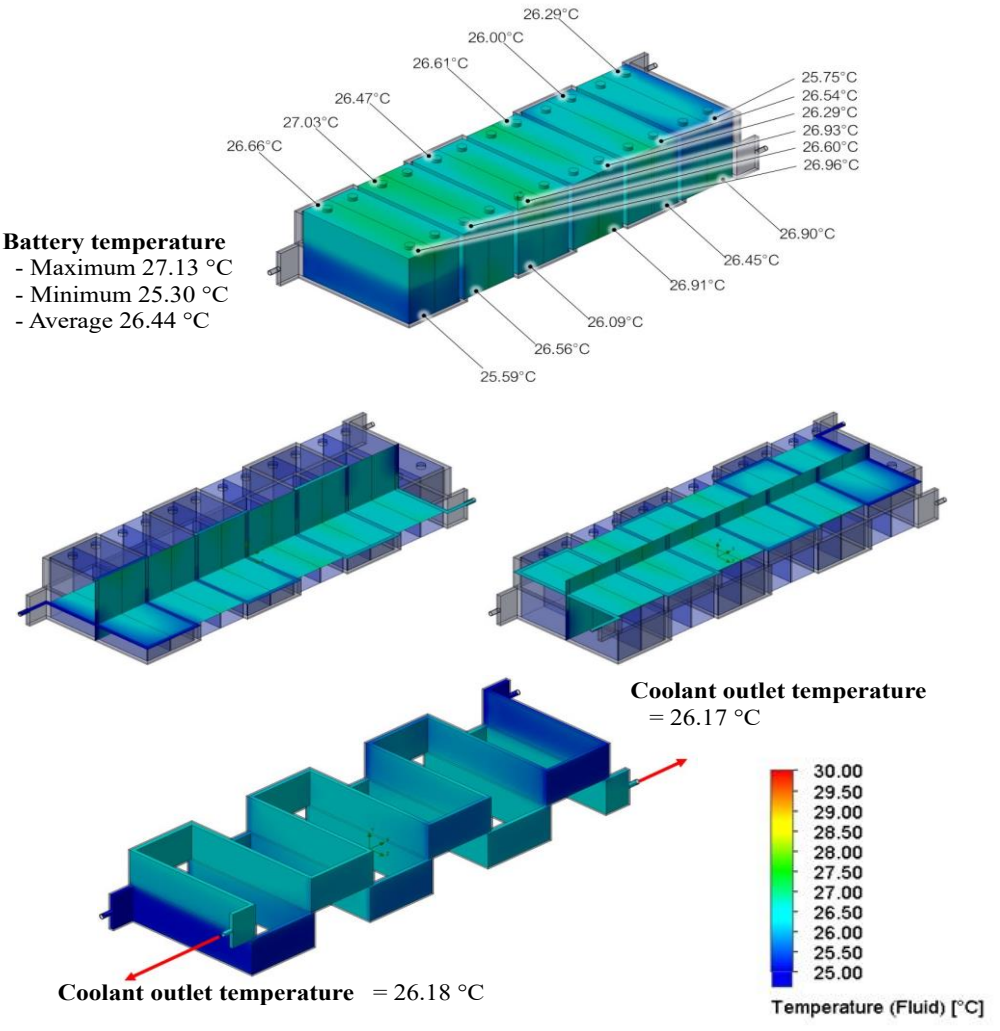

Fig. 10 Variations of the battery module and coolant temperatures for countercurrent flow (Model IV).

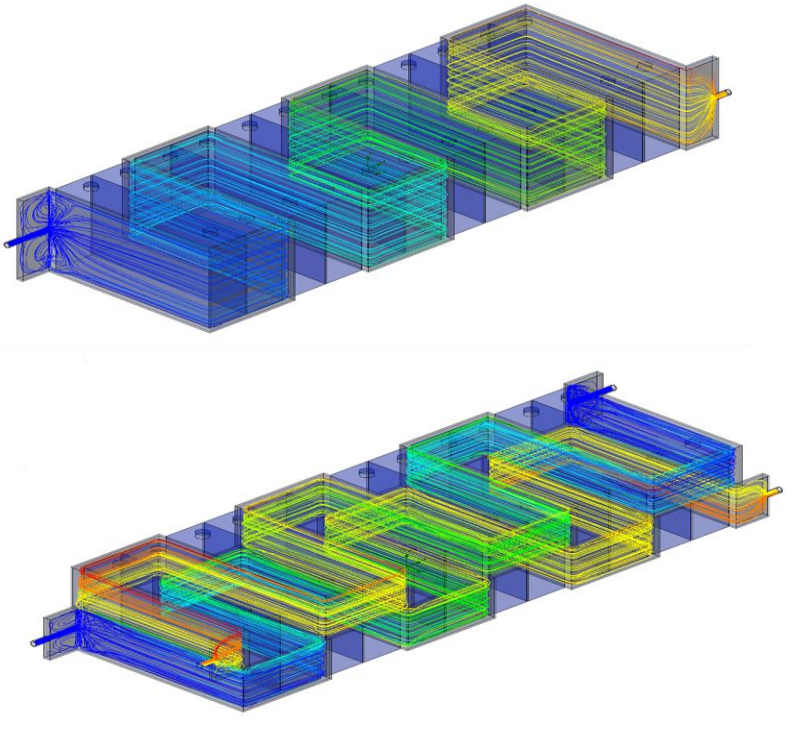

Fig. 11 Streamlines and temperature distributions of coolant (Models I and IV).

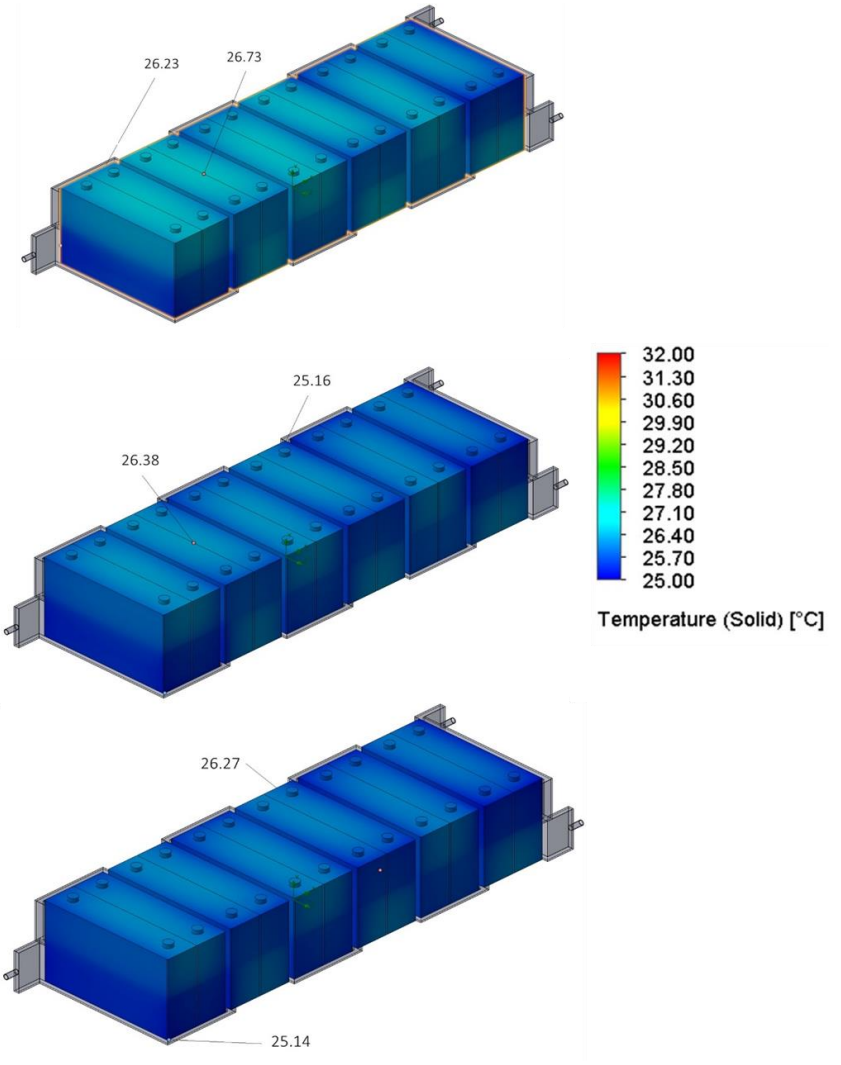

Fig. 12 Variations of battery module temperature (Model IV) for different coolant velocities (0.5, 0.8, 1.0 m/s).

4. Conclusions

The battery cooling system is crucial in its lifetime, performance, and safety risks. The results of the heat transfer behavior of the prismatic $LiFePO_4$ battery pack are presented. The motion of nanoparticles suspended in the base fluid and thermal conductivity significantly affect the battery's heat removal capacity. The predicted results were validated with the measured data, and good agreement was achieved. However, there are some limitations, including excluded interactions between individual scattered phases, the generation of secondary turbulence, and the secondary phase significantly directly impacts turbulence in the primary phase. In the prismatic $LiFePO_4$ battery pack, the highest temperature of the battery pack and the gradient of the cell is still high. This is because the inside of the battery module is not chilled. The uncontrolled increase in temperature and pressure in the battery cells causes the electrolyte to break down, leak, ignite, and explode. A thermal runaway can be initiated. Therefore, the inversed-zigzag cooling channeled flows are proposed, in which the coolant follows along the zigzag flow channel that can chill the central area of the battery pack. The highest temperature values and temperature gradient are different in various cooling models and various thermophysical properties of coolant. It is found that the highest temperatures of the battery packs are 30.26 °C, 30.02 °C, 29.88 °C, 28.67 °C, 27.13 for models I, II(a), II(b), III, and IV, respectively.

Conflict of Interest

There is no conflict of interest.

Supporting Information

Not applicable.

Nomenclatures

C	constant
C_p	specific heat, kJ/(kg °C)
f	friction factor
G	particle-particle interaction modulus, Pa

g gravity acceleration, m/s^2
h heat transfer coefficient, W/(m^2 °C)
I supplied current, ampere
k turbulent kinetic energy, m^2/s^2
p pressure, N/m^2
Q generated heat, W
q heat flux, W/m^2
Re Reynolds number
T temperature, °C
$\boldsymbol{V}$ voltage, V
V velocity, m/s

Greek symbols

ρ density, kg/m^3
ϕ volume fraction
(ρc_p)heat capacity
μ viscosity, kg/ms
β friction coefficient, kg/m^{3}s
λ thermal conductivity, kW/(m °C)
ε dissipation kinetic energy, m^2/s^3

Subscripts

al aluminum
b battery
c convective
coo coolant
dr drift
drag drag
i interface
in inlet
m mixture
out outlet
OCV open circuit voltage
p particle
pw relative velocity
w the base fluid
T temperature, °C
t turbulent

Acronyms

AC air conditioning
BTMS battery thermal management system
C-rate discharge/charge rate relative to maximum capacity
EV electric vehicle
HEV hybrid electric vehicle
Ni-Cd nickel cadmium
NREL National Renewable Energy Laboratory
PCM phase change material
PV/T photovoltaic thermal panel
Li-ion lithium ion

References

[1] J. Garche, E. Karden, P. T. Moseley, D. A. J. Rand, Preface. Lead-Acid Batteries for Future Automobiles. Amsterdam: Elsevier, 2017: xxvii-xxviii, doi: 10.1016/b978-0-444-63700-0.05001-7.

[2] G. J. May, A. Davidson, B. Monahov, Lead batteries for utility energy storage: a review, *Journal of Energy Storage*, 2018, **15**, 145-157, doi: 10.1016/j.est.2017.11.008.

[3] M. P. Indukala, B. M. Mathew, A study on electric vehicle battery, *International Journal of Research Engineering and Technology*, 2019, **6**, 309-314.

[4] K. T. Chau, Y. S. Wong, C. C. Chan, An overview of energy sources for electric vehicles, *Energy Conversion and Management*, 1999, **40**, 1021-1039, doi: 10.1016/s0196-8904(99)00021-7.

[5] Y. Chen, J. W. Evans, Heat transfer phenomena in lithium/polymer-electrolyte batteries for electric vehicle application, *Journal of the Electrochemical Society*, 1993, **140**, 1833-1838, doi: 10.1149/1.2220724.

[6] G.-H. Kim, A. Pesaran, Battery thermal management design modeling, *World Electric Vehicle Journal*, 2007, **1**, 126-133, doi: 10.3390/wevj1010126.

[7] A. Tenno, R. Tenno, T. Suntio, Evaluation of VRLA battery under overcharging: model for battery testing, *Journal of Power Sources*, 2002, **111**, 65-82, doi: 10.1016/s0378-7753(02)00276-8.

[8] A. A. Pesaran, Battery thermal models for hybrid vehicle simulations, *Journal of Power Sources*, 2002, **110**, 377-382, doi: 10.1016/s0378-7753(02)00200-8.

[9] S. Baazouzi, N. Feistel, J. Wanner, I. Landwehr, A. Fill, K. P. Birke, Design, properties, and manufacturing of cylindrical Li-ion battery cells—a generic overview, *Batteries*, 2023, **9**, 309, doi: 10.3390/batteries9060309.

[10] S. Sirikasemsuk, S. Wiriyasart, P. Naphon, Review Thermal management system of battery for electrical vehicles, *SWU Engineering Journal*, 2021, **16**, 93-107.

[11] D. W. Lee, Development of BLDC motor and multi-blade fan for HEV battery cooling system, *International Journal of Automotive Technology*, 2014, **15**, 1101-1106, doi: 10.1007/s12239-014-0114-7.

[12] Z. Ling, F. Wang, X. Fang, X. Gao, Z. Zhang, A hybrid thermal management system for lithium ion batteries combining phase change materials with forced-air cooling, *Applied Energy*, 2015, **148**, 403-409, doi: 10.1016/j.apenergy.2015.03.080.

[13] X. M. Xu, R. He, Research on the heat dissipation performance of battery pack based on forced air cooling, *Journal of Power Sources*, 2013, **240**, 33-41, doi: 10.1016/j.jpowsour.2013.03.004.

[14] H. Sun, R. Dixon, Development of cooling strategy for an air cooled lithium-ion battery pack, *Journal of Power Sources*, 2014, **272**, 404-414, doi: 10.1016/j.jpowsour.2014.08.107.

[15] D. C. Erb, S. Kumar, E. Carlson, I. M. Ehrenberg, S. E. Sarma, Analytical methods for determining the effects of lithium-ion cell size in aligned air-cooled battery packs, *Journal of Energy Storage*, 2017, **10**, 39-47, doi: 10.1016/j.est.2016.12.003.

[16] S. Hong, X. Zhang, K. Chen, S. Wang, Design of flow configuration for parallel air-cooled battery thermal management system with secondary vent, *International Journal of Heat and Mass Transfer*, 2018, **116**, 1204-1212, doi: 10.1016/j.ijheatmasstransfer.2017.09.092.
[17] Y. Xie, Y. Liu, M. Fowler, M.-K. Tran, S. Panchal, W. Li, Y. Zhang, Enhanced optimization algorithm for the structural design of an air-cooled battery pack considering battery lifespan and consistency, *International Journal of Energy Research*, 2022, **46**, 24021-24044, doi: 10.1002/er.8700.
[18] A. Mevawalla, Y. Shabeer, M. K. Tran, S. Panchal, M. Fowler, R. Fraser, Thermal modelling utilizing multiple experimentally measurable parameters, *Batteries*, 2022, **8**, 147, doi: 10.3390/batteries8100147.
[19] S. Pagaria, N. Naik, D. S. Chiniwar, N. Sooriyaperakasam, U. Rathee, Simulation of smarter battery management system and charging for electrical vehicle application, *Journal of Green Engineering*, 2020, **10**, 5365-5379.
[20] X. Jiang, Y. Chen, X. Meng, W. Cao, C. Liu, Q. Huang, N. Naik, V. Murugadoss, M. Huang, Z. Guo, The impact of electrode with carbon materials on safety performance of lithium-ion batteries: a review, *Carbon*, 2022, **191**, 448-470, doi: 10.1016/j.carbon.2022.02.011.
[21] H. M. Ali, Thermal management systems for batteries in electric vehicles: a recent review, *Energy Reports*, 2023, **9**, 5545-5564, doi: 10.1016/j.egyr.2023.04.359.
[22] A. A. Miaari, H.M. Ali, Batteries temperature prediction and thermal management using machine learning: an overview, *Energy Reports*, 2023, **10**, 2277-2305, doi: 10.1016/j.egyr.2023.08.043.
[23] A. M. Bayomy, M. Z. Saghir, T. Yousefi, Electronic cooling using water flow in aluminum metal foam heat sink: experimental and numerical approach, *International Journal of Thermal Sciences*, 2016, **109**, 182-200, doi: 10.1016/j.ijthermalsci.2016.06.007.
[24] B. C. Choi, Thermodynamic analysis of a transcritical CO_2 heat recovery system with 2-stage reheat applied to cooling water of internal combustion engine for propulsion of the 6800 TEU container ship, *Energy*, 2016, **107**, 532-541, doi: 10.1016/j.energy.2016.03.116.
[25] Z. Rao, Y. Zhang, S. Wang, Energy saving of power battery by liquid single-phase convective heat transfer, *Energy Education Science and Technology Part A*, 2012, **30**, 103-112.
[26] S. Panchal, K. Gudlanarva, M.-K. Tran, R. Fraser, M. Fowler, High reynold's number turbulent model for micro-channel cold plate using reverse engineering approach for water-cooled battery in electric vehicles, *Energies*, 2020, **13**, 1638, doi: 10.3390/en13071638.
[27] Z. Rao, Z. Qian, Y. Kuang, Y. Li, Thermal performance of liquid cooling based thermal management system for cylindrical lithium-ion battery module with variable contact surface, *Applied Thermal Engineering*, 2017, **123**, 1514-1522, doi: 10.1016/j.applthermaleng.2017.06.059.
[28] E. Jiaqiang, D. Han, A. Qiu, H. Zhu, Y. Deng, J. Chen, X. Zhao, W. Zuo, H. Wang, J. Chen, Q. Peng, Orthogonal experimental design of liquid-cooling structure on the cooling effect of a liquid-cooled battery thermal management system, *Applied Thermal Engineering*, 2018, **132**, 508-520, doi: 10.1016/j.applthermaleng.2017.12.115.
[29] C. Zhao, W. Cao, T. Dong, F. Jiang, Thermal behavior study of discharging/charging cylindrical lithium-ion battery module cooled by channeled liquid flow, *International Journal of Heat and Mass Transfer*, 2018, **120**, 751-762, doi: 10.1016/j.ijheatmasstransfer.2017.12.083.
[30] T. Zhang, Q. Gao, G. Wang, Y. Gu, Y. Wang, W. Bao, D. Zhang, Investigation on the promotion of temperature uniformity for the designed battery pack with liquid flow in cooling process, *Applied Thermal Engineering*, 2017, **116**, 655-662, doi: 10.1016/j.applthermaleng.2017.01.069.
[31] M. Malik, I. Dincer, M. A. Rosen, M. Mathew, M. Fowler, Thermal and electrical performance evaluations of series connected Li-ion batteries in a pack with liquid cooling, *Applied Thermal Engineering*, 2018, **129**, 472-481, doi: 10.1016/j.applthermaleng.2017.10.029.
[32] S. Sirikasemsuk, S. Wiriyasart, P. Naphon, N. Naphon, Thermal cooling characteristics of Li-ion battery pack with thermoelectric ferrofluid cooling module, *International Journal of Energy Research*, 2021, **45**, 8824-8836, doi: 10.1002/er.6417.
[33] S. Sirikasemsuk, S. Wiriyasart, R. Prurapark, N. Naphon, P. Naphon, Water/nanofluid pulsating flow in thermoelectric module for cooling electric vehicle battery systems, *International Journal of Heat and Technology*, 2021, **39**, 1618-1626, doi: 10.18280/ijht.390525.
[34] S. Sirikasemsuk, S. Wiriyasart, P. Naphon, Experimental investigation of the thermal management system of a battery pack using a thermoelectric air-cooling module, *Heat Transfer*, 2022, **51**, 6384-6402, doi: 10.1002/htj.22596.
[35] P. Naphon, S. Sirikasemsuk, S. Wiriyasart, N. Naphon, Flow direction effects on temperature distribution of li-ion cylindrical battery module with water/ferrofluid as coolants, *Front Heat Mass Transfer*, 2022, **19**, 31, doi: 10.5098/hmt.19.31.
[36] S. Sirikasemsuk, N. Naphon, S. Eiamsa-ard, P. Naphon, Analysis of nanofluid flow and heat transfer behavior of Li-ion battery modules, *International Journal of Heat and Mass Transfer*, 2023, **208**, 124058, doi: 10.1016/j.ijheatmasstransfer.2023.124058.
[37] M. Alipanah, X. Li, Numerical studies of lithium-ion battery thermal management systems using phase change materials and metal foams, *International Journal of Heat and Mass Transfer*, 2016, **102**, 1159-1168, doi: 10.1016/j.ijheatmasstransfer.2016.07.010.
[38] Q. Wang, B. Jiang, B. Li, Y. Yan, A critical review of thermal management models and solutions of lithium-ion batteries for the development of pure electric vehicles, *Renewable and Sustainable Energy Reviews*, 2016, **64**, 106-128, doi: 10.1016/j.rser.2016.05.033.
[39] R. Kizilel, R. Sabbah, J. R. Selman, S. Al-Hallaj, An alternative cooling system to enhance the safety of Li-ion battery packs, *Journal of Power Sources*, 2009, **194**, 1105-1112, doi: 10.1016/j.jpowsour.2009.06.074.

[40] S. Chen, X. Peng, N. Bao, A. Garg, A comprehensive analysis and optimization process for an integrated liquid cooling plate for a prismatic lithium-ion battery module, *Applied Thermal Engineering*, 2019, **156**, 324-339, doi: 10.1016/j.applthermaleng.2019.04.089.
[41] H. Ali, M. S. Kamran, H. M. Ali, S. Imran, Condensation heat transfer enhancement using steam-ethanol mixtures on horizontal finned tube, *International Journal of Thermal Sciences*, 2019, **140**, 87-95, doi: 10.1016/j.ijthermalsci.2019.02.033.
[42] H. M. Ali Recent advancements in PV cooling and efficiency enhancement integrating phase change materials based systems - A comprehensive review, *Solar Energy*, 2020, **197**, 163-198, doi: 10.1016/j.solener.2019.11.075.
[43] C. Liu, P. Du, B. Fang, Z. Li, B. Chen, Z. Rao, Experimental study on a functional microencapsulated phase change material for thermal management, *International Communications in Heat and Mass Transfer*, 2020, **118**, 104876, doi: 10.1016/j.icheatmasstransfer.2020.104876.
[44] V. G. Choudhari, A. S. Dhoble, S. Panchal, Numerical analysis of different fin structures in phase change material module for battery thermal management system and its optimization, *International Journal of Heat and Mass Transfer*, 2020, **163**, 120434, doi: 10.1016/j.ijheatmasstransfer.2020.120434.
[45] Sercan, Yalçın, A CNN-ABC model for estimation and optimization of heat generation rate and voltage distributions of lithium-ion batteries for electric vehicles, *International Journal of Heat and Mass Transfer*, 2022, **199**, 123486, doi: 10.1016/j.ijheatmasstransfer.2022.123486.
[46] G. Karimi, M. Azizi, A. Babapoor, Experimental study of a cylindrical lithium ion battery thermal management using phase change material composites, *Journal of Energy Storage*, 2016, **8**, 168-174, doi: 10.1016/j.est.2016.08.005.
[47] R.-R. Cao, X. Li, S. Chen, H.-R. Yuan, X.-X. Zhang, Fabrication and characterization of novel shape-stabilized synergistic phase change materials based on PHDA/GO composites, *Energy*, 2017, **138**, 157-166, doi: 10.1016/j.energy.2017.07.049.
[48] H.U. Rehman, H.M. Ali, S. Ahmad, M.A. Baluch, Experimental investigation of condensate retention on horizontal pin fin tube with varying pin angle, *Case Studies in Thermal Engineering*, 2020, **17**, 100549, doi: 10.1016/j.csite.2019.100549.
[49] V. Bianco, O. Manca, S. Nardini, Numerical investigation on nanofluids turbulent convection heat transfer inside a circular tube, *International Journal of Thermal Sciences*, 2011, **50**, 341-349, doi: 10.1016/j.ijthermalsci.2010.03.008.
[50] R. Lotfi, Y. Saboohi, A. M. Rashidi, Numerical study of forced convective heat transfer of Nanofluids: comparison of different approaches, *International Communications in Heat and Mass Transfer*, 2010, **37**, 74-78, doi: 10.1016/j.icheatmasstransfer.2009.07.013.
[51] D. Bernardi, E. Pawlikowski, J. Newman, A general energy balance for battery systems, *Journal of the Electrochemical Society*, 1985, **132**, 5-12, doi: 10.1149/1.2113792.
[52] C. Heubner, M. Schneider, C. Lämmel, A. Michaelis, Local heat generation in a single stack lithium ion battery cell, *Electrochimica Acta*, 2015, **186**, 404-412, doi: 10.1016/j.electacta.2015.10.182.
[53] A. Nazari, S. Farhad, Heat generation in lithium-ion batteries with different nominal capacities and chemistries, *Applied Thermal Engineering*, 2017, **125**, 1501-1517, doi: 10.1016/j.applthermaleng.2017.07.126.
[54] M. K. Moraveji, R. M. Ardehali, CFD modeling (comparing single and two-phase approaches) on thermal performance of Al2o3/water nanofluid in mini-channel heat sink, *International Communications in Heat and Mass Transfer*, 2013, **44**, 157-164, doi: 10.1016/j.icheatmasstransfer.2013.02.012.
[55] D. A. Drew, S. L. Passman, Theory of multicomponent fluids, Springer New York, NY, 1999, doi: 10.1007/b97678.
[56] B. C. Pak, Y. I. Cho, Hydrodynamic and heat transfer study of dispersed fluids with submicron metallic oxide particles, *Experimental Heat Transfer*, 1998, **11**, 151-170, doi: 10.1080/08916159808946559.
[57] Y. Xuan, W. Roetzel, Conceptions for heat transfer correlation of nanofluids, *International Journal of Heat and Mass Transfer*, 2000, **43**, 3701-3707, doi: 10.1016/s0017-9310(99)00369-5.
[58] J. C. Maxwell, A Treatise on electricity and magnetism. Clarendon Press, Second Edition, Clarendon Press, UK, 1881.
[59] M. Manninen, V. Taivassalo, S. Kallio, On the Mixture Model for Multiphase Flow, VTT Publications 288, Technical Research Center of Finland, 1996.
[60] L. Schiller, A. Naumann, A drag coefficient correlation, *Zeitschrift des Vereins Deutscher Ingenieure*, 1935, **77**, 318-320.
[61] B. E. Launder, D.B. Spalding, Mathematical models of turbulence. Academic Press, First Edition, 1973.
[62] S. P. Jang, S. U. S. Choi, Cooling performance of a microchannel heat sink with nanofluids, *Applied Thermal Engineering*, 2006, **26**, 2457-2463, doi: 10.1016/j.applthermaleng.2006.02.036.
[63] J. P. Van Doormaal, G. D. Raithby, Enhancements of the simple method for predicting incompressible fluid flows, *Numerical Heat Transfer*, 1984, **7**, 147-163, doi: 10.1080/01495728408961817.
[64] M. Akbarzadeh, T. Kalogiannis, L. Jin, D. Karimi, J. Van Mierlo, M. Berecibar, Experimental and numerical thermal analysis of a lithium-ion battery module based on a novel liquid cooling plate embedded with phase change material, *Journal of Energy Storage*, 2022, **50**, 104673, doi: 10.1016/j.est.2022.104673.
[65] A. A. Pesaran, Battery thermal models for hybrid vehicle simulations, *Journal of Power Sources*, 2002, **110**, 377-382, doi: 10.1016/s0378-7753(02)00200-8.

